ACS MATERIALS LETTERS

www.acsmaterialsletters.org

Magnesium and Aluminum in Contact with Liquid Battery Electrolytes: Ion Transport through Interphases and in the Bulk

Published as part of ACS Materials Letters special issue "Post-Lithium Battery Materials".

Mario Löw, Jonas Grill, Matthias M. May, and Jelena Popovic-Neuber*

Cite This: ACS Materials Lett. 2024, 6, 5120−5127

Read Online

ACCESS | Metrics & More | Article Recommendations | Supporting Information

ABSTRACT: A significant challenge in improving Mg and Al batteries is the limited understanding of the solid electrolyte interphase (SEI) and its evolution under operating conditions. Additionally, the cationic transference number of related electrolytes is crucial for their performance as well as potential dendrite formation yet it is only rarely determined experimentally. Here, we study Al and Mg systems using Grignards as electrolytes for the Mg case and an ionic liquid electrolyte for the Al case. The activation energies associated with ion transport through the SEI suggest that it initially contains a high contribution from liquid pathways for the Mg case and is dense for the Al case, but becomes fully dominated by liquid pathways after a longer contact with the electrolyte. The initial effective Mg cationic transference number of the Grignards is close to zero and increases significantly after only one cyclic voltammetry cycle.

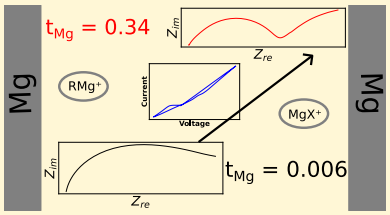

Rechargeable multivalent batteries are promising alternatives to the current lithium-ion batteries.[1−3] For instance, magnesium and aluminum metal batteries could offer a higher volumetric energy density due to their multivalent charge.[3−5] Moreover, these metals are among the most abundant elements on Earth and, therefore, hold the potential for a more sustainable energy storage solution.[6,7] However, understanding and improving the properties of the solid electrolyte interphase (SEI) is crucial for enabling these technologies.[8−10]

For this investigation, we have used two electrolyte systems, including the Gringard electrolytes butylmagnesium chloride (BuMgCl) and ethylmagnesium chloride (EtMgCl), and an ionic liquid doped with aluminum salt, 1-ethyl-3-methylimidazolium chloride-aluminum chloride ([EMImCl]:$AlCl_3$). Grignards are among the first electrolytes used for rechargeable magnesium batteries; they are commercially available and inexpensive.[11,12] Previous electrochemical impedance spectroscopy (EIS) investigations of Grignard electrolytes in symmetric Mg cells showed high total resistances speculated to be related to an adsorption layer present on the Mg anode, containing RMg^+ and RMg· species, stabilized by tetrahydrofuran, as shown by Fourier transform infrared spectroscopy.[11,13,14] Further analysis showed that a native passivation film containing magnesium oxide, magnesium hydroxide, and organic components like carbonates and carboxylates forms on Mg in contact with ambient air.[15,16]

So far, different approaches have been proposed in the recent literature to overcome the ion-blocking passivation layer on top of Mg. One solution is the addition of $LiPF_6$ or $MgBr_2$ to the electrolyte, which was shown to positively affect the SEI formation.[17,18] Another approach is the formation of a so-called artificial SEI. This can be composed of either organic polymers,[19,20] inorganic compounds,[6,21,22] alloys,[23,24] metal−organic frameworks,[25] or 3D scaffolds.[26] Dou et al.[27] investigated the link of the three-dimensional distribution composition to the evolution of the SEI, suggesting that the initial SEI is primarily composed of organic components, leading to electronic leakage, allowing for the decomposition of the electrolyte and continuous growth of a resistive SEI.[27]

[EMImCl]:$AlCl_3$, on the other hand, is a well-established electrolyte for rechargeable aluminium batteries.[28,29] However, it is corrosive to the aluminum, its native oxide, and other components inside the cell.[30−33] For Al metal batteries, the native oxide layer is important since it is dense (Pilling−Bedworth ratio of 1.29)[34] and can suppress the formation of dendrites and confine their existence at the metal/oxide

Received: August 2, 2024
Revised: October 11, 2024
Accepted: October 11, 2024

https://doi.org/10.1021/acsmaterialslett.4c01589
ACS Materials Lett. 2024, 6, 5120−5127

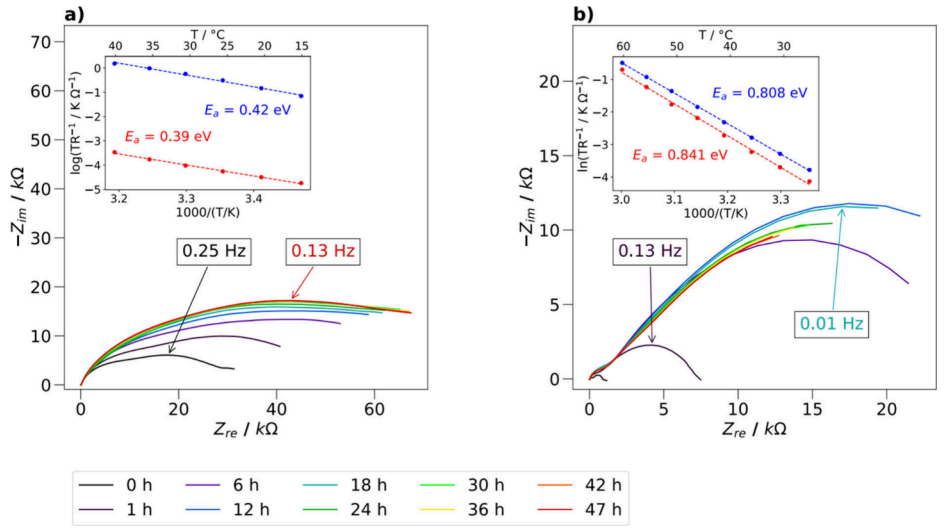

Figure 1. Nyquist plots related to time-dependent EIS measurements of symmetric cells in the 10^7-10^{-2} Hz frequency range: (a) Mg|BuMgCl|Mg and (b) Al|[EMImCl]:$AlCl_3$|Al. Insets: Arrhenius plots and E_a of (a) Mg|BuMgCl|Mg and (b) Al|[EMImCl]:$AlCl_3$|Al. The differently colored Nyquist plots indicate the time in hours from the start of the measurement directly after cell assembly. The red curve shows E_a during increasing temperature; the blue curve shows E_a during decreasing temperature. The activation energy was determined from a freshly assembled cell.

interface.[35−37] Studies of aluminum in contact with [EMImCl]:$AlCl_3$ have shown that the interphase highly depends on the storage conditions and surface properties like roughness and microstructure and may also get dissolved over time.[38,39] However, some corrosion of the native oxide is necessary for adequate cell performance since, otherwise, aluminum cannot be transported over the interface.[35,37] Rahide et al. showed that the presence of Al in an ionic liquid/$AlCl_3$-based electrolyte modifies the surface by creating a beneficial SEI layer containing Al-, Cl-, and N-based compounds.[39]

Further important measurements for insight into the ion transport properties of the electrolyte are related to the determination of the cationic transference numbers and salt diffusion coefficients. This information is essential for understanding dendrite growth and fast charging behavior.[40,41]

The cationic transference number of Grignard electrolytes has yet to be determined. For the related electrolyte C_2H_5MgCl-$((C_2H_5)_2AlCl)_2$/THF, the cationic transference number was determined by potentiometric deposition of Mg in a Hittorf cell. The effective magnesium transference number was found to vary depending on the concentration between 0.19 (0.15 M) and 0.018 (0.4 M).[42] In the case of [EMImCl]:$AlCl_3$, the transference numbers of expected species, $EMIm^+$, $AlCl_4^-$, and Cl^- have already been investigated by Hittorf and other methods, with corresponding effective transference number values of ca. 0.70, 0.30, and 0, respectively.[43−45]

In this letter, we employ in situ EIS to study bulk and interphase ion transport using symmetrical metal cells. This is crucial for the investigation of the SEI since its composition is highly dependent on the environment.[46] This allows us to determine the changes in the electrolyte and SEI resistance over time at conditions as close to open-circuit voltage as possible.[47,48] This type of analysis is well-known in the field of corrosion.[48,49] An ex situ spectroscopy method like X-ray photoelectron spectroscopy would not deliver any necessary information on the morphology of the interphase, while its chemical resolution is also not good enough to determine the distribution of different phases in the SEI, necessary for understanding detailed ion transport properties. Further investigation with operando reflection anisotropy spectroscopy has shown that surfaces created under potential may not be stable and convert within seconds.[50] Furthermore, the analysis of the activation energy of transport (E_a), as well as equivalent circuit development, is essential for elucidating the ion transport in the SEI, especially for determining its possible porosity and dominant liquid conduction pathways.[51] In addition, we use the galvanostatic concentration polarization method combined with EIS to determine the effective cationic transference number and the salt diffusion coefficient.[52] This method coupled with semiblocking electrodes (here, Mg and Al metal) gives access to effective cationic transference numbers of cationic species moving in the direction of positively charged species, which are of relevance for battery performance. For a detailed account of the species that move during galvanostatic polarization with semiblocking electrodes, the reader is directed to consult refs 53−55. Specifically in Grignard electrolytes, Mg does not exist in the form of Mg^{2+} in the electrolyte but only in combination with other ions in the form of RMg^+, RMg·, MgX_2, and MgX^+.[13,14,56−58]

For a better understanding of the ionic transport properties of the SEI and the evolution of the surface over time, the E_a of the ionic conduction in the SEI was determined at the start of the experiment, followed by aging of the cell under open-circuit voltage. Figure 1a shows the evolution of the Nyquist plot over time for the Mg|BuMgCl|Mg system upon application of the EIS perturbation potential. We observe that the total resistance of the semicircle increases in the first 24 h but then reaches saturation. The frequency at the vertex of the semicircle is f_{max} = 0.25 Hz for the initial measurement. This clearly shows that the vertex of the semicircle lies within the range of change transfer reaction (<1 Hz).[59] In addition, the semicircle is also longitudinally distorted. Because of this and according to the observed frequencies, we created an equivalent circuit model containing the resistance of the electrolyte, followed by the SEI's capacity and resistance in parallel, and finally, a Randles circuit for the charge-transfer reaction and diffusion in series (Figure S8 in the Supporting

https://doi.org/10.1021/acsmaterialslett.4c01589
ACS Materials Lett. 2024, 6, 5120−5127

Information (SI)). A comparison of the obtained parameters from the fitting shows that the charge-transfer resistance increases in the first 24 h from 20 to over 50 kΩ and then stays constant. Simultaneously, the double-layer capacity decreases from 450 to 200 μF in the first 24 h and stays relatively constant afterward. The SEI capacity doubles in the same time frame from 4 to 70 μF but then drops to 55 μF for the following 24 h. For the SEI resistance, no clear trend can be observed. The E_a of ionic conduction in the SEI lies between 0.39 and 0.42 eV, which is a clear indication of liquid pathways playing an important role in ionic conduction through the SEI (see the SI for details). This can be concluded since the E_a values of ion transport in some of the best inorganic solid Mg conductors are around 1 eV,[60] while the activation energy of ion transport in Grignard electrolyte is expected to be around 0.1 eV.[61] Similar values have been found in the case of SEIs on Li and Na, where the ion transport in the solid state is generally less sluggish than for Mg-ion conductors.[51] In this case, the situation is even more complex since adsorbed species might be present on the surface of the Mg electrode. However, the ion conduction mechanism through adsorbates is not expected to be different than that through inorganic compounds unless they are solvated. In that case, the liquid ion transport pathways may also be due to these, rather than due to the porous nature of the SEI. The scenario has also been speculated upon by Attias et al.[11] The investigation was repeated for the related Grignard electrolyte EtMgCl. The results are shown in Figure S1. Here, the total resistance of the semicircle also increases with time, and its vertex is around 0.1 Hz, except for the very first semicircle, where it is 3.1 Hz. There is also a long tail in the low-frequency range in this semicircle, which does not occur in the following semicircles, possibly an indication of an electrochemical reaction. Despite the outlier in the first semicircle, the same equivalent circuit was also used to fit this data. Here, the SEI resistance is continuously increased from 10 to 60 kΩ. The capacity of the SEI first jumps from 75 to 95 μF in the first hour and then increases further to 105 μF after 12 h, before it drops again to 80 μF after 47 h. The charge-transfer resistance substantially increases in the first 6 h before fluctuating between 30 and 50 kΩ. The increase in SEI resistance and capacity for both Grignards is assigned to the SEI growth on top of the nondense initial oxide.

The equivalent investigation for aluminum with the [EMImCl]:$AlCl_3$ electrolyte is shown in Figure 1b. Here, a strong increase in the total resistance is observed in the first 6 h, followed by a slighter increase up to 18 h, before it decreases again. The data obtained from [EMImCl]:$AlCl_3$-containing cells were fitted with the previously mentioned equivalent circuit (Figure S8). The reasons for using the same equivalent circuit are, first, the existence of a small semicircle below 1 kΩ and the fact that the vertex of the second semicircle lies with the value of 0.12 Hz. The analysis of the fit shows that the SEI resistance increases strongly in the first 6 h from 200 to 1200 Ω. Afterward, it slightly decreases to around 1000 Ω. In the SEI capacity, there is only a jump in the first hour from 140 to 230 μF before it contentiously increases to 350 μF. The charge-transfer resistance increases in the first 12 h from 0.7 to 40 kΩ and stays relatively constant. The activation energy of ionic conduction in the SEI is around 0.8 eV, indicating a relatively dense SEI.

For aluminum in contact with [EMImCl]:$AlCl_3$, the strong increase of the SEI resistance and capacity in the first few hours, as well as the high E_a of ionic conduction in the SEI at the beginning, is a strong indication of corrosion happening at the interface, leading to a partial removal of the native oxide layer on top of the aluminum.[32,62] Since the native oxide layer is partially removed, the double-layer capacity and the charge-transfer resistance change in this time frame. In situ optical measurements by Guidat et al.[32] show that the partial removal of the native oxide already happens within the first hour after immersion into the electrolyte. This couples well with our investigation.

The magnesium used in the previous section exhibited a blackish surface layer. In the following, this surface was mechanically activated by scratching it with a spatula. Figure 2 compares the EIS response of mechanically activated magnesium with that of the pristine one. A comparison shows that the total resistance of the semicircle of the mechanically activated magnesium is larger than that with native oxide. Fits of both plots are available in Figure S15.

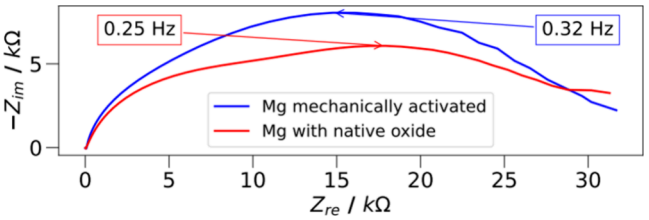

Figure 2. Nyquist plot (10^7–10^{-2} Hz) of Mg with native oxide (red) and mechanically activated Mg (blue) in contact with BuMgCl.

This indicates that the ions face a lower resistance when migrating through the native oxide to the Mg surface than without it. There are two possible explanations for this behavior. A possible explanation could be the change of near-surface composition with exposure to ambient conditions, as the first 10 nm of the Mg surface transform from Mg metal to a mixture of amorphous MgO/OH and then crystalline $Mg(OH)_2$ over a time period of several weeks.[15]

If the crystalline layer performs better with respect to ion transport than the amorphous oxide, its removal by "mechanical activation" would be detrimental to the ion transport through the interphase. This information is crucial for further investigation of magnesium anodes since, in most studies, the native oxide is mechanically removed, expecting improved electrode performance.

The cationic transference numbers for Grignards and the ionic liquid electrolyte were determined by galvanostatic concentration polarization. This type of polarization method was first established[63,64] for the separation of ionic and electronic conductivity and popularized for lithium polymer electrolytes.[65] In contrast to the typical method, we used galvanostatic polarization to determine the initial *IR* response more precisely.[52,66] Therefore, we applied a constant current and recorded the voltage over time until a steady state was reached. In our system, the steady state was reached relatively quickly in under 2 min. The transference number can be calculated via eq 1:

$$t_{pol} = \frac{IR_{tot,0} - IR_{SEI,0}}{U_{\infty} - IR_{SEI,\infty}} \quad (1)$$

https://doi.org/10.1021/acsmaterialslett.4c01589
ACS Materials Lett. 2024, 6, 5120−5127

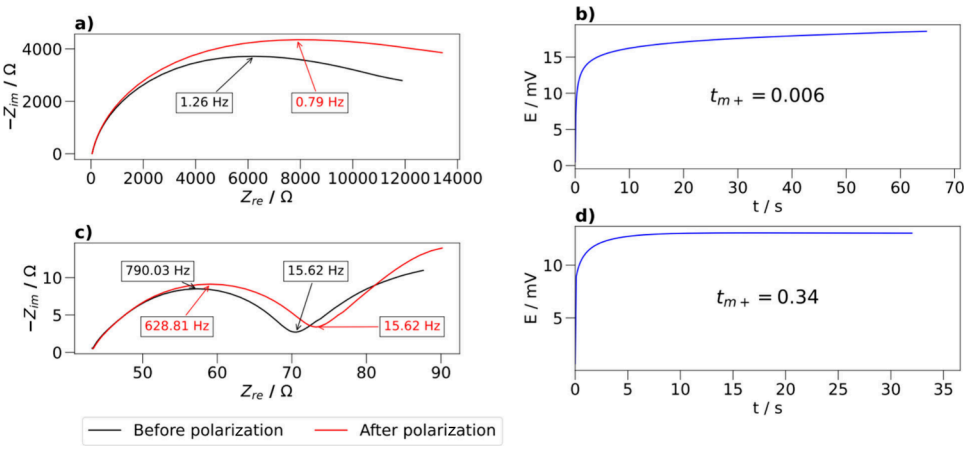

Figure 3. (a) EIS spectra (10^6–10^{-1} Hz) of Mg|BuMgCl|Mg before galvanostatic polarization (black) and after galvanostatic polarization (red). (b) DC polarization curve for $I = 9 \times 10^{-8}$ A. (c) EIS spectra (10^6–10^{-1} Hz) of Mg|BuMgCl|Mg after one CV cycle from −0.5 to 1 V with 10 mV s^{-1} before galvanostatic polarization (black) and after galvanostatic polarization (red). (d) DC polarization curve after the CV cycle for $I = 1 \times 10^{-4}$ A.

where U_∞ is the steady-state voltage, $R_{SEI,0}$ and $R_{SEI,\infty}$ are the resistances of the SEI before and after polarization, respectively, $R_{tot,0}$ is the total resistance before polarization, and I is the applied current during polarization.

In the case of the impedance spectra after cyclic voltammetry (CV), it is also possible to determine the transference number with the low-frequency EIS approach. This considers the electrolyte's resistance (the first intersection between the curve and the x-axis) and the impedance of the polarization (the potential intersection of the right-hand side of the second semicircle):[67]

$$t_{eis} = \frac{1}{1 + \frac{Z_d}{R_{el}}} \tag{2}$$

where Z_d is the impedance of the polarization and R_{el} is the resistance of the electrolyte. In order to obtain the impedance of the polarization from the Nyquist plots in Figure 3, they were fitted with the equivalent circuit described in Figure S8. Before CV, the impedance of the polarization is Z_d = 7625 Ω, and the resistance of the electrolyte is R_{el} = 43.9 Ω; this results in a transference number of $t_{EIS,Mg}$ = 0.0057. After CV, the transference number is $t_{EIS,Mg}$ = 0.37 (Z_d = 72.69 Ω and R_{el} = 43.16 Ω).

Figure 3 shows the Nyquist plot and concentration polarization of BuMgCl in contact with magnesium before and after one CV cycle. The total resistance of the BuMgCl-containing cell is relatively high, over 10 kΩ (Figure 3a). Also, the resulting effective cationic transference number is very small, $t_{Mg,eff}$ = 0.006 (Figure 3b). However, both bulk and interfacial properties change abruptly after only one CV cycle between -0.5 and 1 V (vs Mg). The resistance is significantly reduced to less than 90 Ω, and two semicircles can now be observed. The most striking change, however, is in the cationic transference number, which is significantly increased to $t_{Mg,eff}$ = 0.34. Similar behavior is observed with ethylmagnesium chloride, where the transference number increases from $t_{Mg,eff}$ = 0.004 before CV to 0.41 after CV (see plots in Figure S3). As shown by Benmayza et al.[42] for the C_2H_5MgCl-$((C_2H_5)_2AlCl)_2$ electrolyte, the low t_{Mg} is expected at higher concentrations due to the lower mobility of the Mg dimer ion and the presence of many counter- and non-magnesium ions.[42] The change of $t_{Mg,eff}$ upon the CV run, with values of the same order of magnitude as those of well-performing lithium liquid electrolytes, indicates a drastic change of magnesium speciation or its mobility. We have shown that this is possible in lithium liquid electrolytes with a high concentration of neutral ion pairs.[55] Here, we can speculate that the increase of cationic transference number is again a consequence of the interplay between the existence of a high number of noncharged ion pairs and a smaller amount of magnesium in the positively charged aggregates.

The cationic transference number was also determined for [EMImCl]:$AlCl_3$ (Figure S6). Here, a value of $t_{Al,eff}$ = 0.063 was observed, which aligns well with a previous study showing a nonexistent effective transport of aluminum and dominant aluminum transport in negatively charged species, t_{AlCl^-} = 0.30 ± 0.02.[43] In this case, after one CV cycle, the $t_{Al,eff}$ decreases even further to 0.0004, indicating a nonbeneficial change in speciation/mobility. In addition to the effective transference number values, it is also possible to extract the ambipolar diffusion coefficient of all species, D^δ, from the polarization curve at short polarization times. Therefore, eq 3 was used:

$$D^\delta = \frac{L^2}{\tau^\delta \pi^2} \tag{3}$$

where L is the thickness of the separator and τ^δ is the time constant. The latter can be obtained by plotting the voltage of the chronopotentiometry from the polarization experiment against the square root of the time, with the slope of the linear part being the polarization constant (Figure 4). For BuMgCl, a value of $D^\delta = 1.2 \times 10^{-7}$ cm^2 s^{-1} was obtained, and for

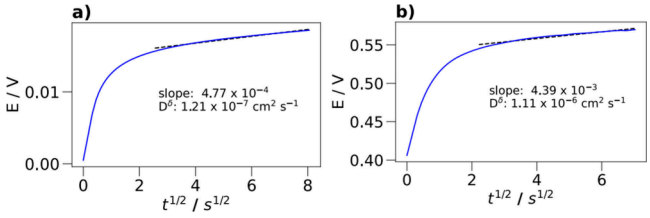

Figure 4. Ambipolar salt diffusion coefficient obtained from the square-root dependence of time vs voltage in the short-time regime of DC polarization for (a) BuMgCl and (b) [EMIm-Cl]:$AlCl_3$.

https://doi.org/10.1021/acsmaterialslett.4c01589
ACS Materials Lett. 2024, 6, 5120−5127

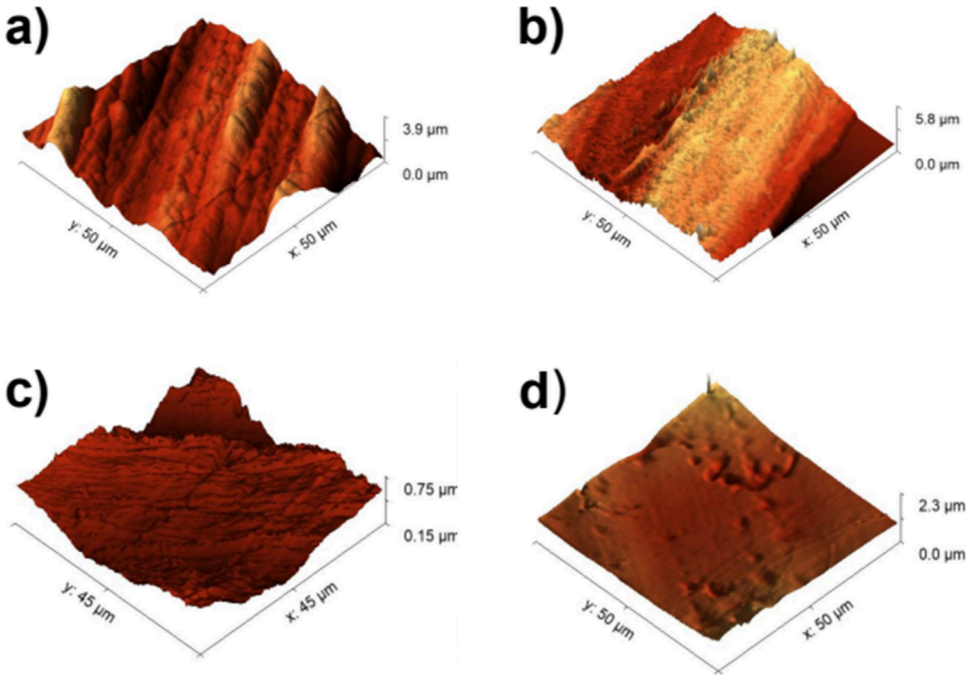

Figure 5. AFM images of the Mg-foil and Al-foil. (a) Fresh Mg-foil with native oxide. (b) Mg-foil with native oxide after prolonged contact with the BuMgCl electrolyte. (c) Fresh Al-foil and (d) Al-foil after prolonged contact with the [EMImCl]:$AlCl_3$ electrolyte.

EtMgCl, a value of $D^{\delta} = 1.0 \times 10^{-7}$ cm^2 s^{-1} was obtained. For [EMImCl]:$AlCl_3$, salt diffusion coefficient of 1.1×10^{-6} cm^2 s^{-1} was observed, which is an order of magnitude higher compared to the literature value.[68]

For a better understanding of the processes taking place at the electrode−electrolyte interphase, both magnesium and aluminum were investigated with atomic force microscopy (AFM) in the pristine state as well as after prolonged contact with their respective electrolyte. The AFM images in Figure 5a,b show that the roughness of the magnesium electrode remained unchanged. The pristine foil displays grooves, likely resulting from the manufacturing process. The small spikes observed on the electrode after contact with the BuMgCl electrolyte are probably scanning artifacts. For Al, Figure 5c,d shows that the surface roughness increases after prolonged contact. Here, two processes take place; first, small Al structures are removed due to the corrosiveness of the electrolyte. Second, pitting of the surface and salt deposition from the electrolyte can also occur, leading to areas with higher differential altitudes and features of several micrometers in height. This results in a smoother surface with some additional larger structures. We also quantitatively assessed the surface roughness of both surfaces. For the pristine Al-foil, the root-mean-square value for the roughness is 197 nm, while it is 309 nm after prolonged contact with the electrolyte. Compared to the research by Sabi et al.,[33] where no effective change was observed after 18 h of exposure, we experience an increase in the surface roughness while immersing the sample in the electrolyte.

In summary, the evolution of the interphase of symmetric Mg and Al cells with Grignard and [EMImCl]:$AlCl_3$ as respective electrolytes was investigated by EIS. The evolution of the shape of the Nyquist plots and the E_a associated with ion transport through the SEI indicates that the interphase of magnesium and aluminum is dominated by liquid ion transport pathways for magnesium and is already dense in the case of aluminum at the beginning. Liquid ion transport pathways remain relevant for both interphases over time. AFM investigations additionally show that the roughness of the magnesium surface stays about the same while immersed in the Grignard. However, the roughness increases for Al due to the electrolyte's corrosiveness. For the Grignards, the cationic transference number increase from $t_{Mg,eff} = 0.006$ to $t_{Mg,eff} = 0.34$ after only one CV cycle, indicating a profound change in the transport properties of the electrolyte. For [EMImCl]:$AlCl_3$, the cationic transference number stays relatively low with $t_{Al,eff} = 0.063$ and does not increase upon electrochemical cycling.

The drastic change in the transference numbers of the Grignard electrolytes after one cycle is related to the change in speciation and/or the related mobility of species. Nuclear magnetic resonance and infrared measurements might be beneficial here. Further, we want to encourage the community of multivalent batteries to do more research on the transference numbers of their electrolytes since they are one of the critical factors for improving electrolytes, as shown by us in this work by a simple setup.

■ ASSOCIATED CONTENT

Data Availability Statement

The data that support the findings of this study are openly available on Zenodo at https://doi.org/10.5281/zenodo.12750755.

Supporting Information

The Supporting Information is available free of charge at https://pubs.acs.org/doi/10.1021/acsmaterialslett.4c01589.

Experimental details, time-dependent Nyquist plots of EtMgCl, transference number measurements of EtMgCl and [EMImCl]:$AlCl_3$, additional CVs, and tables with the fitting values and plots of the Nyquist plots presented in the paper (PDF)

https://doi.org/10.1021/acsmaterialslett.4c01589
ACS Materials Lett. 2024, 6, 5120−5127

AUTHOR INFORMATION

Corresponding Author

Jelena Popovic-Neuber − *University of Stavanger, Faculty of Science and Technology, Department of Energy and Petroleum Engineering, 4021 Stavanger, Norway;* orcid.org/0000-0001-6618-4306; Email: jelena.popovic-neuber@uis.no

Authors

Mario Löw − *Universität Ulm, Institute of Theoretical Chemistry, 89081 Ulm, Germany*

Jonas Grill − *University of Stavanger, Faculty of Science and Technology, Department of Energy and Petroleum Engineering, 4021 Stavanger, Norway*

Matthias M. May − *Universität Tübingen, Institute of Physical and Theoretical Chemistry, 72076 Tübingen, Germany; Universität Ulm, Institute of Theoretical Chemistry, 89081 Ulm, Germany;* orcid.org/0000-0002-1252-806X

Complete contact information is available at: https://pubs.acs.org/10.1021/acsmaterialslett.4c01589

Author Contributions

CRediT: **Mario Löw** conceptualization, data curation, formal analysis, investigation, validation, visualization, writing - original draft, writing - review & editing; **Jonas Grill** conceptualization, data curation, formal analysis, investigation, methodology, validation, writing - original draft, writing - review & editing; **Matthias M. May** conceptualization, data curation, formal analysis, funding acquisition, investigation, resources, supervision, validation, writing - original draft, writing - review & editing; **Jelena Popovic-Neuber** conceptualization, data curation, formal analysis, funding acquisition, investigation, methodology, resources, supervision, validation, visualization, writing - original draft, writing - review & editing.

Notes

The authors declare no competing financial interest.

ACKNOWLEDGMENTS

This work was funded by Deutsche Forschungsgemeinschaft (DFG, German Research Foundation) under Germany's Excellence Strategy - EXC 2154 - Project 390874152, DFG Project 434023472 and institutional funding by University of Stavanger. Mats Ingdal, Dagfinn Sødenaa Sleveland, and Ola Ketil Siqveland are thanked for their laboratory support.

REFERENCES

(1) Liu, F.; Wang, T.; Liu, X.; Fan, L.-Z. Challenges and Recent Progress on Key Materials for Rechargeable Magnesium Batteries. *Adv. Energy Mater.* **2021**, *11*, 2000787.

(2) Elia, G. A.; Kravchyk, K. V.; Kovalenko, M. V.; Chacón, J.; Holland, A.; Wills, R. G. An overview and prospective on Al and Al-ion battery technologies. *J. Power Sources* **2021**, *481*, 228870.

(3) Gupta, S. K.; Vishwakarma, J.; Srivastava, A. K.; Dhand, C.; Dwivedi, N. Aluminum batteries: Opportunities and challenges. *Energy Storage Mater.* **2024**, *70*, 103538.

(4) Faegh, E.; Ng, B.; Hayman, D.; Mustain, W. E. Practical assessment of the performance of aluminium battery technologies. *Nat. Energy* **2021**, *6*, 21−29.

(5) Liang, Y.; Dong, H.; Aurbach, D.; Yao, Y. Current status and future directions of multivalent metal-ion batteries. *Nat. Energy* **2020**, *5*, 646−656.

(6) Zhang, X.; Lv, R.; Tang, W.; Li, G.; Wang, A.; Dong, A.; Liu, X.; Luo, J. Challenges and Opportunities for Multivalent Metal Anodes in Rechargeable Batteries. *Adv. Funct. Mater.* **2020**, *30*, 2004187.

(7) Lee, E.-S.; Huh, S.-H.; Lee, S.-H.; Yu, S.-H. On the Road to Stable Electrochemical Metal Deposition in Multivalent Batteries. *ACS Sustain. Chem. Eng.* **2023**, *11*, 2014−2032.

(8) Popovic, J. In *Nanomaterials for Electrochemical Energy Storage*; Raccichini, R., Ulissi, U., Eds.; Elsevier, 2021; p 327−359.

(9) Liu, X.; Wang, G.; Lv, Z.; Du, A.; Dong, S.; Cui, G. A Perspective on Uniform Plating Behavior of Mg Metal Anode: Diffusion Limited Theory versus Nucleation Theory. *Adv. Mater.* **2023**, *36*, 2306395.

(10) Tang, K.; Du, A.; Dong, S.; Cui, Z.; Liu, X.; Lu, C.; Zhao, J.; Zhou, X.; Cui, G. A Stable Solid Electrolyte Interphase for Magnesium Metal Anode Evolved from a Bulky Anion Lithium Salt. *Adv. Mater.* **2020**, *32*, 1904987.

(11) Attias, R.; Dlugatch, B.; Chae, M. S.; Goffer, Y.; Aurbach, D. Changes in the interfacial charge-transfer resistance of Mg metal electrodes, measured by dynamic electrochemical impedance spectroscopy. *Electrochem. Commun.* **2021**, *124*, 106952.

(12) Lu, Z.; Schechter, A.; Moshkovich, M.; Aurbach, D. On the electrochemical behavior of magnesium electrodes in polar aprotic electrolyte solutions. *J. Electroanal. Chem.* **1999**, *466*, 203−217.

(13) Aurbach, D. Magnesium Deposition and Dissolution Processes in Ethereal Grignard Salt Solutions Using Simultaneous EQCM-EIS and In Situ FTIR Spectroscopy. *Electrochem. Solid-State Lett.* **1999**, *3*, 31.

(14) Aurbach, D.; Turgeman, R.; Chusid, O.; Gofer, Y. Spectroelectrochemical studies of magnesium deposition by in situ FTIR spectroscopy. *Electrochem. Commun.* **2001**, *3*, 252−261.

(15) Fotea, C.; Callaway, J.; Alexander, M. R. Characterisation of the surface chemistry of magnesium exposed to the ambient atmosphere. *Surf. Interface Anal.* **2006**, *38*, 1363−1371.

(16) Newberg, J. T.; Starr, D. E.; Yamamoto, S.; Kaya, S.; Kendelewicz, T.; Mysak, E. R.; Porsgaard, S.; Salmeron, M. B.; Brown, G. E.; Nilsson, A.; Bluhm, H. Formation of hydroxyl and water layers on MgO films studied with ambient pressure XPS. *Surf. Sci.* **2011**, *605*, 89−94.

(17) Xie, Y.; Song, H.; Ye, S.; Tian, F.; Xie, J.; Lei, D.; Wang, C. Hybrid solid electrolyte interphases formed in conventional carbonate electrolyte enable high-voltage and ultrastable magnesium metal batteries. *J. Energy Chem.* **2023**, *78*, 315−324.

(18) Chinnadurai, D.; Lieu, W. Y.; Kumar, S.; Yang, G.; Li, Y.; Seh, Z. W. A Passivation-Free Solid Electrolyte Interface Regulated by Magnesium Bromide Additive for Highly Reversible Magnesium Batteries. *Nano Lett.* **2023**, *23*, 1564−1572.

(19) Häcker, J.; Rommel, T.; Lange, P.; Zhao-Karger, Z.; Morawietz, T.; Biswas, I.; Wag-ner, N.; Nojabaee, M.; Friedrich, K. A. Magnesium Anode Protection by an Organic Artificial Solid Electrolyte Interphase for Magnesium-Sulfur Batteries. *ACS Appl. Mater. Interfaces.* **2023**, *15*, 33013−33027.

(20) Son, S.-B.; Gao, T.; Harvey, S. P.; Steirer, K. X.; Stokes, A.; Norman, A.; Wang, C.; Cresce, A.; Xu, K.; Ban, C. An artificial interphase enables reversible magnesium chemistry in carbonate electrolytes. *Nat. Chem.* **2018**, *10*, 532−539.

(21) Luo, L.; Yang, X.; Gao, Z.; Li, X.; Xu, J.; Zhang, Y.; Deng, R.; Huang, G.; Wang, J.; Pan, F. Overcoming passivation in rechargeable magnesium batteries: Artificial solid electrolyte interface for enhanced anode functionality. *Electrochim. Acta* **2024**, *478*, 143815.

(22) Li, X.; Gao, T.; Han, F.; Ma, Z.; Fan, X.; Hou, S.; Eidson, N.; Li, W.; Wang, C. Reducing Mg Anode Overpotential via Ion Conductive Surface Layer Formation by Iodine Additive. *Adv. Energy Mater.* **2018**, *8*, 1701728.

(23) Wan, B.; Dou, H.; Zhao, X.; Wang, J.; Zhao, W.; Guo, M.; Zhang, Y.; Li, J.; Ma, Z.-F.; Yang, X. Three-Dimensional Magnesiophilic Scaffolds for Reduced Passivation toward High-Rate Mg Metal Anodes in a Noncorrosive Electrolyte. *ACS Appl. Mater. Interfaces.* **2020**, *12*, 28298−28305.

(24) Lv, R.; Guan, X.; Zhang, J.; Xia, Y.; Luo, J. Enabling Mg metal anodes rechargeable in conventional electrolytes by fast ionic transport interphase. *Natl. Sci. Rev.* **2020**, *7*, 333−341.

(25) Zhang, Y.; Li, J.; Zhao, W.; Dou, H.; Zhao, X.; Liu, Y.; Zhang, B.; Yang, X. Defect-Free Metal−Organic Framework Membrane for

Precise Ion/Solvent Separation toward Highly Stable Magnesium Metal Anode. *Adv. Mater.* **2022**, *34*, 2108114.
(26) Song, Z.; Zhang, Z.; Du, A.; Dong, S.; Li, G.; Cui, G. Uniform Magnesium Electrodeposition via Synergistic Coupling of Current Homogenization, Geometric Confinement, and Chemisorption Effect. *Adv. Mater.* **2021**, *33*, 2100224.
(27) Dou, H.; Zhao, X.; Zhang, Y.; Zhao, W.; Yan, Y.; Ma, Z.-F.; Wang, X.; Yang, X. Revisiting the degradation of solid/electrolyte interfaces of magnesium metal anodes: Decisive role of interfacial composition. *Nano Energy* **2021**, *86*, 106087.
(28) Ferrara, C.; Dall'Asta, V.; Berbenni, V.; Quartarone, E.; Mustarelli, P. Physicochemical Characterization of AlCl3−1-Ethyl-3-methylimidazolium Chloride Ionic Liquid Electrolytes for Aluminum Rechargeable Batteries. *J. Phys. Chem. C* **2017**, *121*, 26607−26614.
(29) Borozdin, A.; Elterman, V.; Shevelin, P. Y.; Yolshina, L. Electrochemical behavior of aluminum in 1-ethyl-3-methylimidazolium chloroaluminate ionic liquids. *Electrochim. Acta* **2024**, *490*, 144265.
(30) Craig, B.; Schoetz, T.; Cruden, A.; Ponce de Leon, C. Review of current progress in non-aqueous aluminium batteries. *Renew. Sustain. Energy Rev.* **2020**, *133*, 110100.
(31) Chang, J.-K.; Chen, S.-Y.; Tsai, W.-T.; Deng, M.-J.; Sun, I.-W. Electrodeposition of aluminum on magnesium alloy in aluminum chloride (AlCl3)−1-ethyl-3-methylimidazolium chloride (EMIC) ionic liquid and its corrosion behavior. *Electrochem. Commun.* **2007**, *9*, 1602−1606.
(32) Guidat, M.; Rahide, F.; Löw, M.; Kim, J.; Ehrenberg, H.; Dsoke, S.; May, M. M. In Situ Monitoring of the Al(110)-[EMImCl]: AlCl3 Interface by Reflection Anisotropy Spectroscopy. *Batter. Supercaps* **2024**, *7*, e202300394.
(33) Sabi, N.; Palanisamy, K.; Rahide, F.; Daboss, S.; Kranz, C.; Dsoke, S. Surface Properties-Performance Relationship of Aluminum Foil as Negative Electrode for Rechargeable Aluminum Batteries. *Batter. Supercaps* **2023**, *6*, e202300298.
(34) Xu, C.; Gao, W. Pilling-Bedworth ratio for oxidation of alloys. *Mater. Res. Innov.* **2000**, *3*, 231−235.
(35) Chen, H.; Xu, H.; Zheng, B.; Wang, S.; Huang, T.; Guo, F.; Gao, W.; Gao, C. Oxide Film Efficiently Suppresses Dendrite Growth in Aluminum-Ion Battery. *ACS Appl. Mater. Interfaces.* **2017**, *9*, 22628−22634.
(36) Das, S. K.; Mahapatra, S.; Lahan, H. Aluminium-ion batteries: developments and challenges. *J. Mater. Chem. A* **2017**, *5*, 6347−6367.
(37) Choi, S.; Go, H.; Lee, G.; Tak, Y. Electrochemical properties of an aluminum anode in an ionic liquid electrolyte for rechargeable aluminum-ion batteries. *Phys. Chem. Chem. Phys.* **2017**, *19*, 8653−8656.
(38) Loaiza, L. C.; Lindahl, N.; Johansson, P. Initial Evolution of Passivation Layers in Non-Aqueous Aluminium Batteries. *J. Electrochem. Soc.* **2023**, *170*, No. 030512.
(39) Rahide, F.; Palanisamy, K.; Flowers, J. K.; Hao, J.; Stein, H. S.; Kranz, C.; Ehrenberg, H.; Dsoke, S. Modification of Al Surface via Acidic Treatment and its Impact on Plating and Stripping. *ChemSusChem* **2023**, *17*, e202301142.
(40) Bai, P.; Li, J.; Brushett, F. R.; Bazant, M. Z. Transition of lithium growth mechanisms in liquid electrolytes. *Energy Environ. Sci.* **2016**, *9*, 3221−3229.
(41) Zheng, J.; Engelhard, M. H.; Mei, D.; Jiao, S.; Polzin, B. J.; Zhang, J.-G.; Xu, W. Electrolyte additive enabled fast charging and stable cycling lithium metal batteries. *Nat. Energy* **2017**, *2*, 17012.
(42) Benmayza, A.; Ramanathan, M.; Arthur, T. S.; Matsui, M.; Mizuno, F.; Guo, J.; Glans, P.-A.; Prakash, J. Effect of Electrolytic Properties of a Magnesium Organohaloaluminate Electrolyte on Magnesium Deposition. *J. Phys. Chem. C* **2013**, *117*, 26881−26888.
(43) Dymek, C. J.; King, L. A. Transport Numbers in Molten Aluminum Chloride-1-Methyl-3-Ethylimidazolium Chloride Mixtures. *J. Electrochem. Soc.* **1985**, *132*, 1375−1380.
(44) Hussey, C. L.; Oye, H. A. Transport Numbers in Molten Acidic Aluminum Chloride-1-Methyl-3-Ethylimidazolium Chloride: Their Relationship to EMF Measurements in Chloroaluminate Melts. *J. Electrochem. Soc.* **1984**, *131*, 1621−1625.
(45) Hussey, C. L.; Sanders, J. R.; Oye, H. A. Transport Numbers in the Basic Aluminum Chloride-1-Methyl-3-Ethylimidazolium Chloride Ionic Liquid. *J. Electrochem. Soc.* **1985**, *132*, 2156−2158.
(46) Villevieille, C. Interfaces and Interphases in Batteries: How to Identify and Monitor Them Properly Using Surface Sensitive Characterization Techniques. *Adv. Mater. Interfaces* **2022**, *9*, 2101865.
(47) Nojabaee, M.; Küster, K.; Starke, U.; Popovic, J.; Maier, J. Solid Electrolyte Interphase Evolution on Lithium Metal in Contact with Glyme-Based Electrolytes. *Small* **2020**, *16*, 2000756.
(48) Popovic, J. Solid Electrolyte Interphase Growth on Mg Metal Anode: Case Study of Glyme-Based Electrolytes. *Energy Technol.* **2021**, *9*, 2001056.
(49) Gomes, M. P.; Costa, I.; Pébère, N.; Rossi, J. L.; Tribollet, B.; Vivier, V. On the corrosion mechanism of Mg investigated by electrochemical impedance spectroscopy. *Electrochim. Acta* **2019**, *306*, 61−70.
(50) Löw, M.; Guidat, M.; Kim, J.; May, M. M. The interfacial structure of InP(100) in contact with HCl and H_2SO_4 studied by reflection anisotropy spectroscopy. *RSC Adv.* **2022**, *12*, 32756−32764.
(51) Lim, K.; Fenk, B.; Popovic, J.; Maier, J. Porosity of Solid Electrolyte Interphases on Alkali Metal Electrodes with Liquid Electrolytes. *ACS Appl. Mater. Interfaces.* **2021**, *13*, 51767−51774.
(52) Popovic, J.; Hasegawa, G.; Moudrakovski, I.; Maier, J. Infiltrated porous oxide monoliths as high lithium transference number electrolytes. *J. Mater. Chem. A* **2016**, *4*, 7135−7140.
(53) Maier, J. Concentration Polarization of Salt-Containing Liquid Electrolytes. *Adv. Funct. Mater.* **2011**, *21*, 1448−1455.
(54) Maier, J. Salt concentration polarization of liquid electrolytes and determination of transport properties of cations, anions, ion pairs and ion triples. *Electrochim. Acta* **2014**, *129*, 21−27.
(55) Popovic, J.; Höfler, D.; Melchior, J. P.; Münchinger, A.; List, B.; Maier, J. High Lithium Transference Number Electrolytes Containing Tetratriflylpropene's Lithium Salt. *J. Phys. Chem. Lett.* **2018**, *9*, 5116−5120.
(56) Aurbach, D.; Schechter, A.; Moshkovich, M.; Cohen, Y. On the Mechanisms of Reversible Magnesium Deposition Processes. *J. Electrochem. Soc.* **2001**, *148*, A1004.
(57) Gofer, Y.; Turgeman, R.; Cohen, H.; Aurbach, D. XPS Investigation of Surface Chemistry of Magnesium Electrodes in Contact with Organic Solutions of Organochloroaluminate Complex Salts. *Langmuir* **2003**, *19*, 2344−2348.
(58) Maddegalla, A.; Kumar, Y.; Chakrabarty, S.; Glagovsky, Y.; Schmerling, B.; Fridman, N.; Afri, M.; Aviv, H.; Aurbach, D.; Mukherjee, A.; Bravo-Zhivotovskii, D.; Noked, M. First isolation of solvated $MgCl^+$ species as the sole cations in electrolyte solutions for rechargeable Mg batteries. *Electrochim. Acta* **2023**, *463*, 142869.
(59) Lazanas, A. C.; Prodromidis, M. I. Electrochemical Impedance Spectroscopy-A Tutorial. *ACS Meas. Sci. Au* **2023**, *3*, 162−193.
(60) Roedern, E.; Kühnel, R.-S.; Remhof, A.; Battaglia, C. Magnesium Ethylenediamine Borohydride as Solid-State Electrolyte for Magnesium Batteries. *Sci. Rep.* **2017**, *7*, 46189.
(61) Sheha, E. Ion transport properties of magnesium bromide/dimethyl sulfoxide non-aqueous liquid electrolyte. *J. Adv. Res.* **2016**, *7*, 29−36.
(62) Natishan, P. M.; O'Grady, W. E. Chloride Ion Interactions with Oxide-Covered Aluminum Leading to Pitting Corrosion: A Review. *J. Electrochem. Soc.* **2014**, *161*, C421−C432.
(63) Hebb, M. H. Electrical Conductivity of Silver Sulfide. *J. Chem. Phys.* **1952**, *20*, 185−190.
(64) Wagner, C. Galvanische Zellen mit festen Elektrolyten mit gemischter Stromleitung. *Z. Elektrochem.* **1956**, *60*, 4−7.
(65) Evans, J.; Vincent, C. A.; Bruce, P. G. Electrochemical measurement of transference numbers in polymer electrolytes. *Polymer* **1987**, *28*, 2324−2328.
(66) Popovic, J. Insights into Cationic Transference Number Values and Solid Electrolyte Interphase Growth in Liquid/Solid Electrolytes

https://doi.org/10.1021/acsmaterialslett.4c01589
ACS Materials Lett. 2024, 6, 5120−5127

for Potassium Metal Batteries. *ACS Phys. Chem. Au.* **2022**, *2*, 490−495.
(67) Ravn Sørensen, P.; Jacobsen, T. Conductivity, charge transfer and transport number—an ac-investigation of the polymer electrolyte LiSCN-poly(ethyleneoxide). *Electrochim. Acta* **1982**, *27*, 1671−1675.
(68) Peng, Y.; Shinde, P. S.; Reddy, R. G. Diffusion coefficient and nucleation density studies on electrochemical deposition of aluminum from chloroaluminate ionic liquid electrolytes. *J. Electroanal. Chem.* **2021**, *895*, 115363.

https://doi.org/10.1021/acsmaterialslett.4c01589
ACS Materials Lett. 2024, 6, 5120−5127